JOURNAL OF MATERIALS SCIENCE 7 (1972) 1175–1191

The fracture energy of carbon-fibre reinforced glass

D. C. PHILLIPS
Process Technology Division, AERE, Harwell, Didcot, Berks, UK

The fracture energy of carbon-fibre reinforced glass has been measured by the work of fracture technique, using specimens of varied geometry. Meaningful material properties were obtained only when crack propagation was controlled throughout failure. The work of fracture (γ_F) depended on strain-rate and fibre volume fraction, and was typically ~ 3 kJm^{-2} for a 40 vol % specimen. Variations of work of fracture due to strain-rates have been related to the microstructure of the fracture surfaces and estimates have been obtained of the fibre-matrix interfacial shear stress during pull-out. Approximate estimates have been made of the fracture initiation energy (γ_I) by fracture mechanics analyses. γ_I was less than γ_F and no strain-rate sensitivity was detected. An attempt has been made to explain γ_I in terms of the initial rate of release of strain energy during fibre fracture.

1. Introduction

Glasses and ceramics are usually susceptible to fracture under conditions of thermal or mechanical shock. Further, although high tensile strengths can frequently be achieved by careful fabrication techniques, these strengths are lost when the surfaces of the materials are damaged. These effects are largely a consequence of the low fracture energies of glasses and ceramics, which are a result of the absence of the energy absorption mechanisms which occur in materials which are intuitively considered to be tough. Thus, for example, in metals fracture is preceded by plastic deformation and in wood fracture occurs by fibrous tearing, processes which can absorb much energy. Typically ceramics display fracture energies within the range 3 to 50 Jm^{-2} while for metals and wood the values are usually in excess of 10^4 Jm^{-2} [1].

One method of increasing the fracture energy of a ceramic is to incorporate within it fibres to produce a composite material. Recent work has shown how this has been achieved with carbon fibres in glass, glass-ceramic, magnesia and alumina [2]. In particular, some mechanical properties of carbon-fibre reinforced Pyrex glass (CFRG), containing aligned continuous fibres, have been published and it was shown that the fracture energy is a few kJm^{-2} for crack propagation perpendicular to the fibre direction in a composite containing about 50 vol% of fibre [3].

There are essentially two different principles employed in measuring fracture energy. One involves measuring the total energy introduced into a specimen during fracture and in this category fall, for example, the work of fracture technique and Charpy impact. The other involves measuring the initial rate of strain-energy release at fracture and in this category are the techniques of fracture-mechanics analysis. Davidge and Tappin [4] have shown that the fracture energies of several homogeneous brittle materials (alumina, perspex, glass and graphite) are not the same at all stages in the fracture process. They defined fracture energy (γ), which they called effective surface energy, as the work done to create unit area of new fracture face, not taking into account fine-scale surface irregularities – the same definition is used here. In particular, they suggested that the fracture-mechanics analysis techniques measure a fracture energy γ_I pertaining to the initiation of fracture, while the work of fracture technique measures γ_F, a value of fracture energy averaged over the whole of the fracture process. The differences between γ_I and γ_F were not large in their materials and the explanation of the differences was that crack initiation is more difficult than propagation in the glass-like materials because of a multiplicity of surface crack sources, while the reverse is true in materials containing many volume crack sources as in graphite.

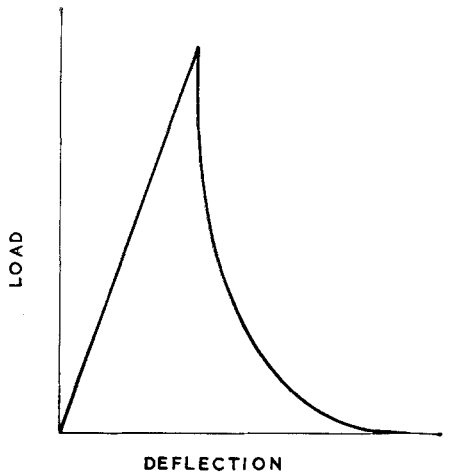

Figure 1 Schematic representation of a load-deflection curve obtained during controlled fracture.

The work of fracture technique, developed by Tattersall and Tappin [1] and Nakayama [5] for measuring the fracture energy of brittle materials, is frequently used to measure the fracture energy of fibre composites. The technique involves deforming a specimen in three-point bending until it has completely fractured. If fracture proceeds in a non-catastrophic manner as shown in Fig. 1, all the stored elastic energy in the specimen-machine system at the onset of failure is, in principle, converted into fracture energy as the load decreases to zero. To obtain controlled failure in a brittle material such as a ceramic, it is necessary to use a specimen with a deep notch cut into the tensile face so that the total stored elastic energy at failure is smaller than the total energy required for fracture. It is also an advantage to use a hard testing machine which does not store much elastic energy. The work of fracture is then

$$\gamma_F = \frac{\text{Energy under load-deflection curve}}{2 \times \text{specimen cross-sectional area}}.$$

Because of the high works of fracture of fibre composites, it is frequently unnecessary to insert a notch to obtain a non-catastrophic failure of the form shown in Fig. 1 [3].

Techniques based on the initial rate of strain energy release measure γ_I which is the value of fracture energy used in the Griffith equation and which is one of the parameters which defines the strength of the material in the presence of flaws. γ_I can be measured from the load at failure of a specimen if its geometry has been related to the Griffith-Irwin criterion of failure by a suitable fracture-mechanics analysis, and in general, for any given geometry

$$\gamma_I = F(P_m, C_{ij})$$

where P_m is the load at failure and C_{ij} are the elastic constants of the material [6]. Alternatively, γ_I may be obtained by determining the variation of specimen stiffness (k) with crack area and relating this to the load or deflection at failure for a given crack area [7]. Provided certain conditions are satisfied, γ_I is related to the plane strain, linear elastic fracture mechanics, opening mode fracture toughness parameter G_{Ic} by $2\gamma_I = G_{Ic}$. Apart from the obvious conditions of plane-strain and opening-crack mode, it is necessary for the crack to be sharp. When the crack is not sharp, or plane-strain conditions are not satisfied, $\gamma_I > G_{Ic}/2$.

The high values of γ of CFRG, of a few kJm^{-2}, were obtained using the work of fracture technique. In this paper a closer examination is made of the work of fracture technique as applied to composites, and an attempt is made to understand the relationship between γ_F and γ_I and their physical meaning in CFRG. Only fracture on a plane perpendicular to the fibres is considered, as this is characteristic of the composite system, whereas fracture on planes parallel to the fibres tends to be characteristic of the matrix.

2. Experimental

CFRG was fabricated by a hot-pressing technique. Some details of this process, and the mechanical properties of material produced in this way, have been described elsewhere [2, 3, 8, 9]. The composite material has reproducible properties which are largely determined by the properties of the carbon fibre before its incorporation into a matrix. The specimens used in this work were made in several separate batches, under otherwise identical conditions, and the properties of the carbon fibre, and microstructural details of the composites are presented in Table I. Fibre-volume fractions and open and closed porosities were obtained from a series of density and burn-out measurements. Fibre strengths and elastic moduli were obtained from whole-tow and single fibre measurements respectively.

Flexural strengths and interlaminar shear strengths, where quoted, have been obtained from measurements in three-point bending.

TABLE I Specimen details

Specimen	Fibre		Composite					
	Strength MNm^{-2}	Modulus GNm^{-2}	Volume percentage (vol %)				Mean strengths (MNm^{-2})	
			Fibre	Glass	Open porosity	Closed porosity	Flexural	Shear
LP301	1940	405	39.6	59.0	0.4	1.0	798	70
LP355	1130	313	36.2	63.3	0.4	0.1	498	69
L473	1780	319	19.8	78.8	0.5	0.9	342	—
L474	1780	319						
L475, L476	1780	319	24.0	74.7	0.6	0.7	408	—
L477, L478	1780	319	31.2	66.6	0.7	1.5	445	—
L479, L480	1780	319	41.4	56.9	1.1	0.6	501	—
L481, L482	1780	319	57.1	35.0	7.9	0	259	—

Specimen cross-sections were 2.5 × 1 mm and the flexural and shear tests were carried out over 30 and 4 mm spans, respectively.

Works of fracture were obtained from specimens of two different geometries: straight-notched specimens as shown in Fig. 2a with a variable notch depth (c); and circumferentially-notched specimens as in Fig. 2b. Both types were fractured over a 40 mm span. The straight-notched specimens were loaded by a single roller, and thus fractured in three-point bending. The circumferentially-notched specimens were loaded by two rollers spaced 12 mm apart, and were thus fractured in four-point bending.

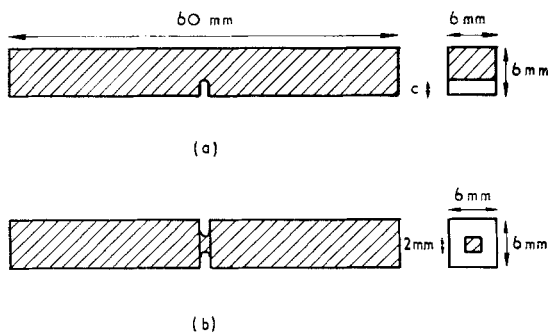

Figure 2 Work of fracture specimens (a) straight-notched (b) circumferentially-notched.

All mechanical testing was carried out on a floor model Instron machine with a 500 kg compressive load cell, at cross-head speeds which are quoted in the text.

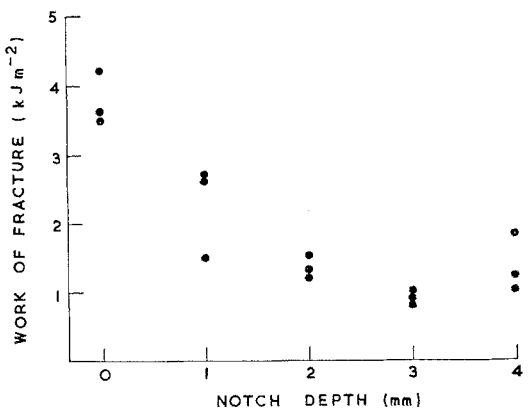

Figure 3 The variation of work of fracture with notch depth for straight-notched specimens of LP355.

3. The fracture of CFRG

3.1. The effect of straight-notch depth

Fig. 3 shows the variation of work of fracture with notch depth for straight-notched specimens of LP355. Representative load-deflection curves are shown in Fig. 4. All the specimens, even those which were un-notched, fractured in a non-catastrophic manner. During fracture, the propagating crack frequently branched into two or more cracks and, because of the material anisotropy did not in general travel perpendicularly to the fibres. This is shown in Fig. 5 which is a photograph of some fractured specimens of

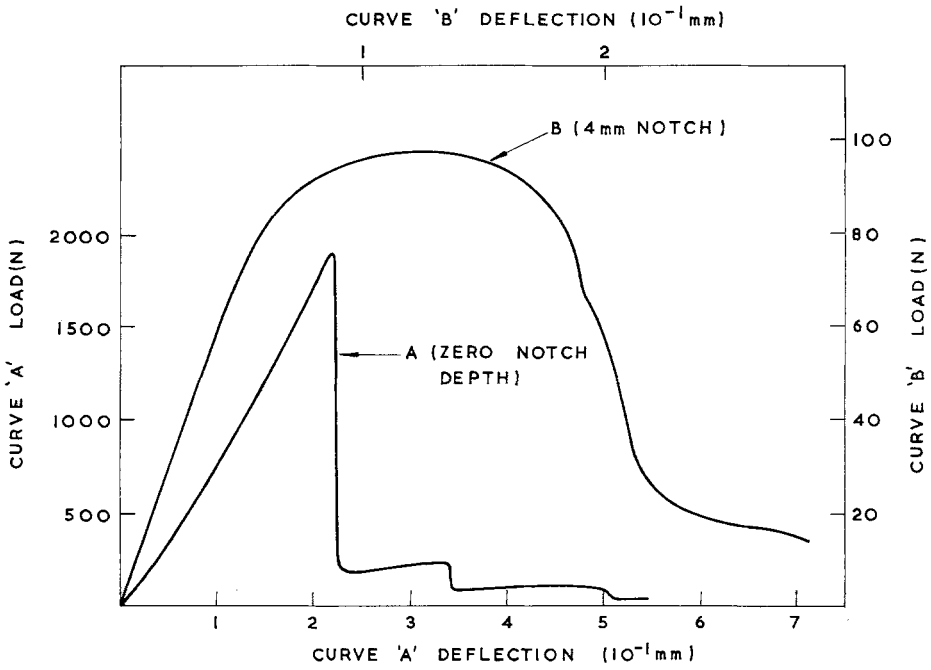

Figure 4 Representative load-deflection curves of straight-notched specimens.

varied notch depth. The work of fracture was calculated by dividing the energy of the integrated load-deflection curve by the total area of fracture projected on to a plane perpendicular to the fibres, that area having been estimated by a microscopic study of the fractured specimens. This procedure effectively ignores the possibility of a significant contribution to the work of fracture from components of crack propagation parallel to the fibres, but takes into account all contributions from branched cracks running perpendicular to the fibres. This is considered permissible within the scope of this paper because the contribution to the total energy from crack propagation parallel to the fibres is relatively very small, work of fracture measurements for fracture parallel to the fibres having yielded values ~ 10 Jm^{-2}. The effect of this procedure, as opposed to dividing by twice the cross-sectional area of the specimen, was to reduce the scatter in work of fracture values at any notch depth, without altering the overall shape of the curve of γ_F versus notch depth in Fig. 3.

Table II shows the mean deflections at failure and Fig. 6 shows the variation of stiffness k with notch depth, where $k = P/\delta$, and P is the load at a deflection δ. All the data presented in this section were obtained at an Instron cross-head speed of 0.5 mm min^{-1}.

TABLE II Mean deflection at failure δ_f, notch depth c and initial crack area A of straight notched γ_F specimens

c (m)	A (m^2)	δ_f (m)
1×10^{-3}	1.2×10^{-5}	1.6×10^{-4}
2×10^{-3}	2.4×10^{-5}	1.2×10^{-4}
3×10^{-3}	3.6×10^{-5}	9.1×10^{-5}
4×10^{-3}	4.8×10^{-5}	7.0×10^{-5}

3.2. Circumferential notches

Fig. 7 is typical of the load-deflection curves obtained with circumferentially notched specimens. It differs from that of most of the straight-notch specimens (Fig. 4) in that after the specimen attained its maximum load, there was no sudden uncontrolled crack propagation as the crack propagated independently of the Instron cross-head displacement. Instead, crack propagation in these specimens was controlled by the motion of the cross-head at all the strain-rates and fibre-volume fractions used in this work.

The works of fracture of these specimens have been calculated by dividing the energy of the

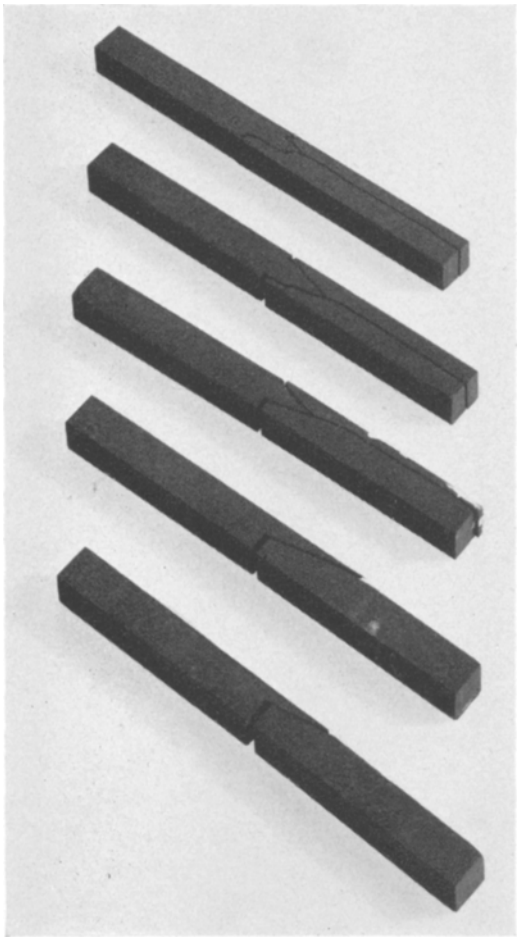

Figure 5 Fractured straight-notch specimens.

integrated load-deflection curve by twice the cross-sectional area of the fractured neck because there was no evidence of significant crack branching.

3.2.1. The effect of strain-rate

Fig. 8 shows the effect of cross-head speed on γ_F for circumferentially notched bars of LP301 and LP355. There is a clear variation of γ_F with strain-rate. Table III shows the stiffness and maximum loads at the fastest and slowest cross-head speeds. Between four and six specimens were used for each of these tests and there is no significant trend of variation of stiffness or maximum load with cross-head speed.

3.2.2. The effect of fibre-volume fraction

Fig. 9 shows the variation of γ_F with fibre volume fraction for circumferentially notched specimens of L473 to L482, obtained at a cross-head speed of 0.5 mm min^{-1}.

3.3. The effect of strain-rate on flexural strength

Table III also shows the mean flexural strengths and stiffnesses of flexural bars of LP301, obtained at two different cross-head speeds. Six specimens were tested at each cross-head speed and there is no significant variation between the two sets.

3.4. The microstructure of fracture

3.4.1. Fracture surfaces

The fracture surfaces of many of these specimen-have been studied by scanning electron microscopy. Circumferentially notched specimens show a clear dependence of length of protruding fibre on strain-rate. For example, Figs. 10a and b are photographs of part of the fracture surfaces of circumferentially notched specimens of LP301 which were fractured at cross-head speeds of 0.05 mm min^{-1} and 10 mm min^{-1} respectively. Fibres protruding from the fracture face of the more rapidly-loaded specimens tend to be

TABLE III Stiffness, maximum loads and maximum stresses at different rates of loading (uncertainties are standard errors)

Specimens and loading rates	Stiffness (Nm^{-1})		Maximum loads (N) or stresses (MNm^{-2})	
	Slow loading (Nm^{-1})	Fast loading (Nm^{-1})	Slow loading	Fast loading
Circumferentially-notched LP301 (0.05 mm min^{-1} and 10.0 mm min^{-1})	$1.1 \pm 0.1 \times 10^6$	$1.2 \pm 0.1 \times 10^6$	167 ± 10 N	144 ± 10 N
Circumferentially-notched LP355 (0.05 mm min^{-1} and 10.0 mm min^{-1})	$1.14 \pm 0.06 \times 10^6$	$1.25 \pm 0.05 \times 10^6$	107 ± 4 N	116 ± 8 N
Flexural bars LP301 (0.05 mm min^{-1} and 20 mm min^{-1})	$5.1 \pm 0.2 \times 10^4$	$5.2 \pm 0.2 \times 10^4$	764 ± 17 MNm^{-2}	771 ± 19 MNm^{-2}

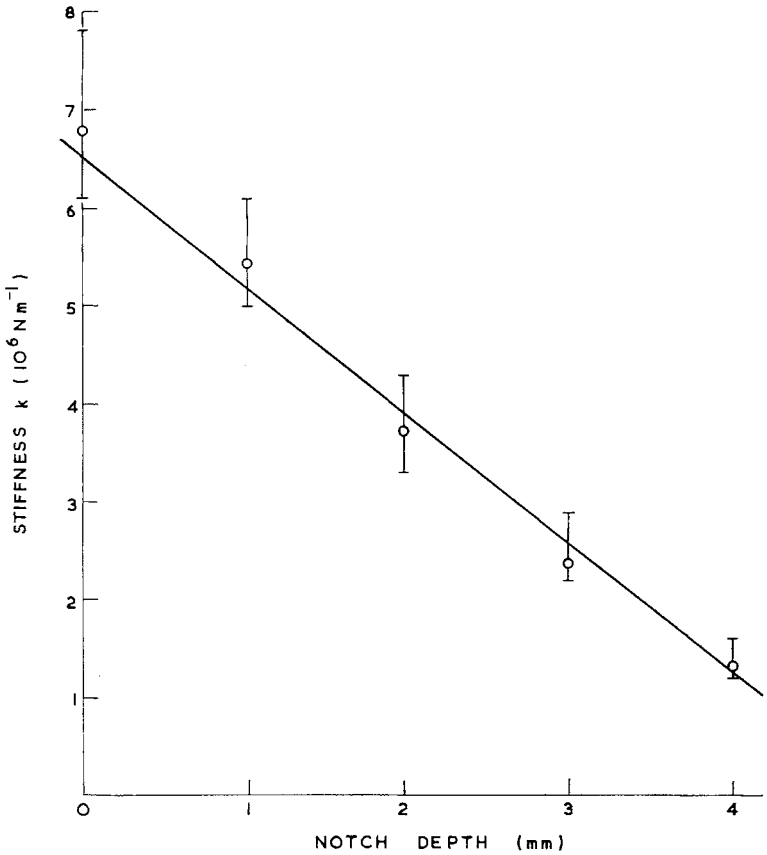

Figure 6 Variation of stiffness with straight-notch depth.

shorter than those of the slower specimens. This effect is shown more quantitatively by the histograms and the mean fibre lengths in Fig. 11. These were obtained from measurements made on the specimens of LP355 whose γ_F variation is shown in Fig. 8. Photographs, similar to Fig. 10, were taken of three different regions of the fracture face of each of two specimens fractured at each of three different strain-rates. Each photograph was taken at the same angle (45° to the fracture face) and the fibres were measured from each photograph.

A Scanning Electron Microscope study was also made of the fracture microstructure of the straight-notched specimens. Many of these failed with the crack propagating at an oblique angle to the fibres so that it was not possible to make comparisons of pull-out lengths; however, some of the un-notched and shallow-notched specimens failed with the crack running in a direction mainly perpendicular to the fibres. The pull-out length of the fibres in the un-notched specimens tended to vary across the fracture face, being shorter at the onset of fracture than at the end. This effect is shown in Figs. 12a and b which are photographs taken at the same angle of different regions of the same fracture surface of an un-notched specimen.

3.4.2. Matrix microcracking

When a CFRG specimen is loaded to failure in tension, microcracking occurs in the matrix at stresses below the ultimate failure stress [8] of the composite, because the failure strain of the glass matrix is lower than that of the carbon fibre. It can be shown [8] that the matrix microcracking tends to occur at a regular spacing t which is related to the fibre-matrix interfacial shear strength, the matrix strength and the fibre-volume fraction. The effect of strain-rate on t has been determined by measuring the microcrack spacing of the polished tensile and side

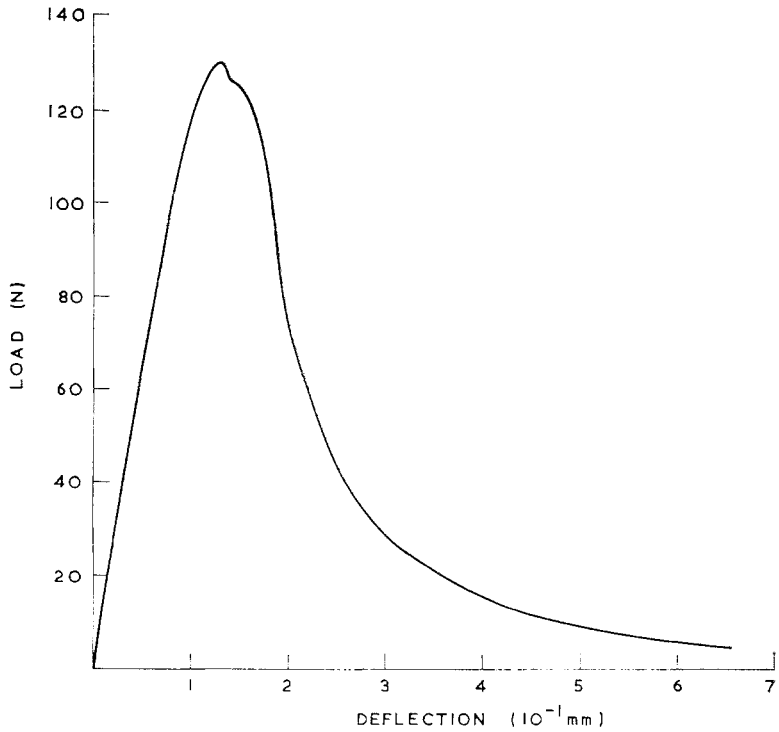

Figure 7 A load-deflection curve of a circumferentially-notched specimen.

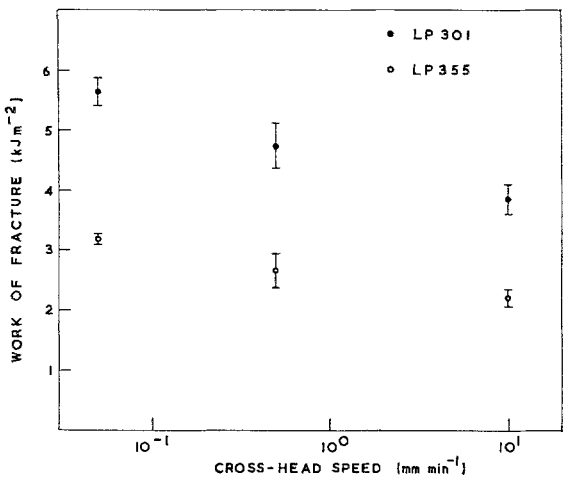

Figure 8 The variation with cross-head speed of γ_F of circumferentially-notched specimens of LP301 and LP355.

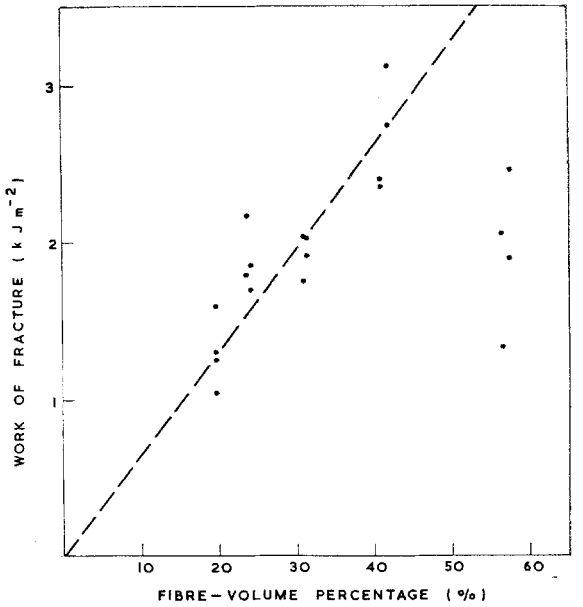

Figure 9 The variation of γ_F with fibre-volume fraction.

faces of the flexural bars of LP301, which were fractured at varied strain-rates. Fig. 13 is a photograph of a region of microcracking. The difficulty in measuring the crack spacing is that in practice the cracks do not extend continuously across the surface of the specimen and it is therefore necessary to find regions where a number of cracks lie across a common perpen-

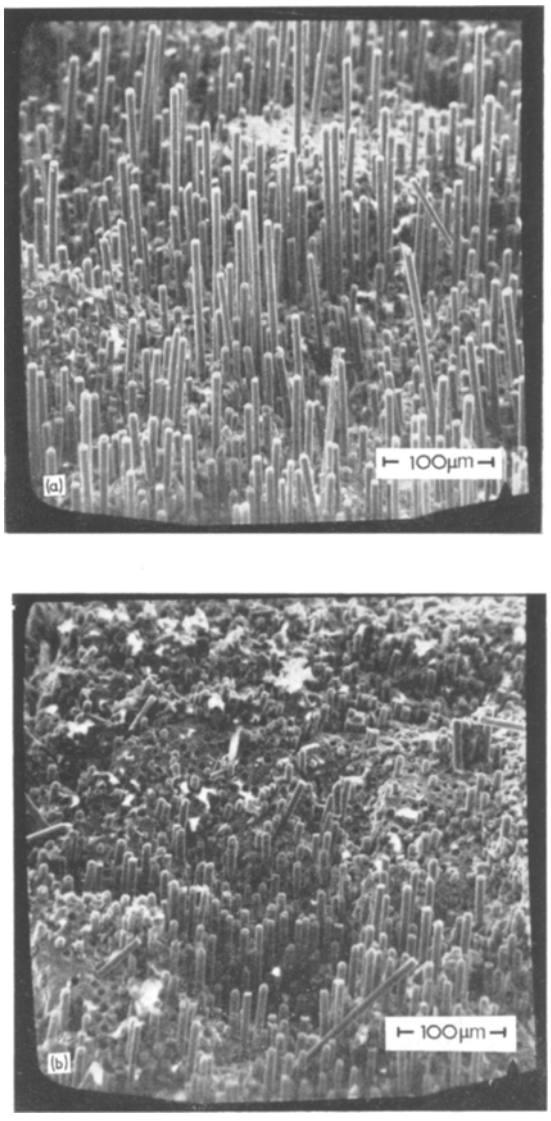

Figure 10 The fracture surfaces of circumferentially-notched specimens of LP301. (a) fractured at 0.05 mm min^{-1}. (b) 10 mm min^{-1}.

dicular line. This results in an uncertainty in measured values of t which is displayed by the histograms of crack spacing shown in Fig. 14. The mean crack spacings were 89 $\pm$ 6 μm and 90 $\pm$ 12 μm for cross-head speeds of 0.05 mm min^{-1} and 20 mm min^{-1} respectively.

4. Discussion

4.1. Work of fracture

The dependence of work of fracture on notch depth (Fig. 3) observed in the straight notch experiments is similar to that observed by Davidge and Tappin in brittle homogeneous materials. High works of fracture are obtained when the notch is shallow and the load-deflection curve is similar to curve A in Fig. 4. On testing such specimens, the load initially falls very rapidly at the onset of failure as the crack or cracks propagate at speeds which are not controlled by the Instron cross-head velocity, and then slow down, further crack propagation being controlled by the movement of the cross head. As the notch depth is increased, fracture becomes progressively more controlled, the initial rapid fall-off of load becomes smaller, and the work of fracture decreases. At deep notch depth, a completely-controlled fracture is obtained as demonstrated by a load-deflection curve of the form of curve B in Fig. 4 in which all stages of fracture are controlled by the Instron cross-head movement.

A completely-controlled fracture is also obtained with circumferentially-notched specimens. The works of fracture obtained from these specimens depend on the rapidity with which they are fractured and are related to the microstructure of the fracture surfaces. The more rapidly such a specimen is fractured, the lower its work of fracture and the shorter the mean length of protruding fibre. The lengths of fibres protruding from the fracture faces of the un-notched and shallow, straight-notched specimens of LP355, were very much less than those of even the rapidly-fractured circumferentially-notched specimens, although their works of fracture were higher. However, the variation of length of fibre across the fracture face of an un-notched specimen was qualitatively similar to the observed dependence of length on fracture speed in circumferentially-notched material. As Figs. 12a and b show, the protruding length is shorter at the onset of failure when the crack is propagating rapidly, than towards the end of fracture when it is propagating slowly. On theoretical grounds, higher works of fracture due to fibre pull-out are associated with larger pull-out lengths. These facts suggest that the high works of fracture obtained at shallow notch depths, when failure is of the form of curve A in Fig. 4, are not material properties but are anomolously high due to loss of energy from the system during the uncontrolled stage of fracture. Meaningful values of γ_F are obtained when failure is completely controlled, as in a circumferentially-notched specimen test. A similar conclusion was obtained

by Davidge and Tappin for brittle homogeneous materials.

Work of fracture generally increases with fibre-volume fraction as is expected, and the decrease in work of fracture at the high volume fractions is undoubtedly associated with the high matrix porosities which also lead to decreased flexural strength.

4.2. Fracture initiation energies

There are several reasons for believing that in CFRG the energy for fracture initiation (γ_I) is not the same as γ_F, but is smaller. For any fixed geometry, the energy of crack initiation γ_I is a function of the maximum load at failure and the elastic properties of the material. γ_F values obtained from circumferentially-notched speci-

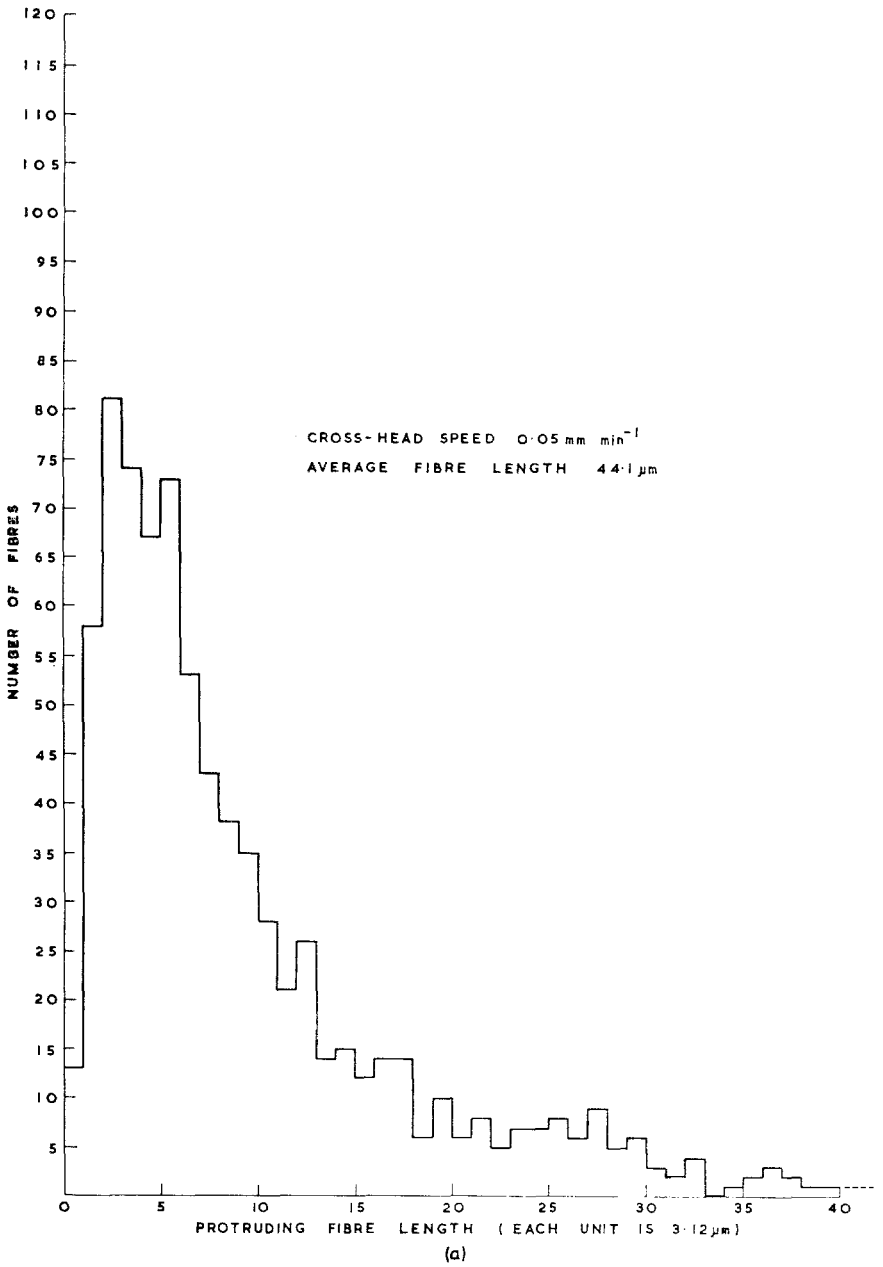

Figure 11 a, b and c are histograms of protruding lengths of fibres.

mens vary quite substantially with loading rate, increasing by almost 50% when the cross-head speed decreases from 10 mm min^{-1} to 5×10^{-2} mm min^{-1}. However, Table III shows that within experimental uncertainty there is no significant variation in the maximum loads or stiffness of these specimens, or of the flexural bars, over the same range of cross-head speeds suggesting no significant variation of γ_I. Further, if typical values of γ_F, strength (σ) and effective elastic modulus (E_{eff}) for a 40 to 50 vol% specimen (3 kJm^{-2}, 700 MNm^{-2} and 55 GNm^{-2} respectively) are inserted in the Griffith equation

$$\sigma = \left\{\frac{2E_{eff}\gamma}{\pi c}\right\}^{1/2} \quad (1)$$

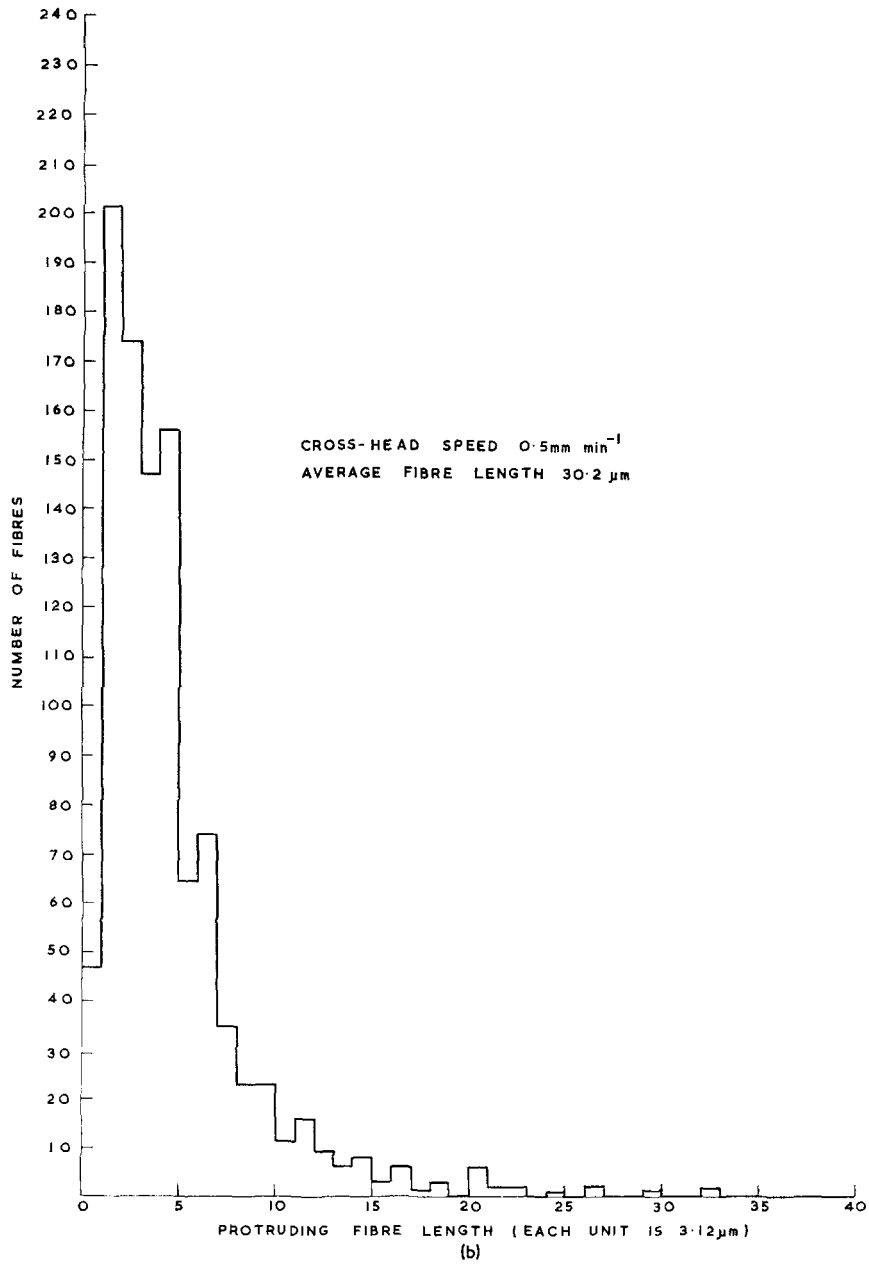

Figure 11

the calculated flaw size c is about 0.25 mm. A flaw could be a crack in the composite, or an equivalent region of broken or misoriented fibres. However, this flaw size is unreasonably large as strengths of 700 MNm^{-2} are commonly obtained off specimens of 2 × 1 mm cross-section. Flaws of 0.25 mm would be readily apparent on microscopic examination and do not in general occur. The maximum size of flaw which might occur and not be identified would be, at most, about 0.1 mm, and this suggests that $\gamma_I \lesssim 1\ kJm^{-2}$.

Values of γ_I have been calculated from the data obtained from the single-notched specimens. Analytical solutions, appropriate to a fracture-mechanics analysis, exist for elastically-

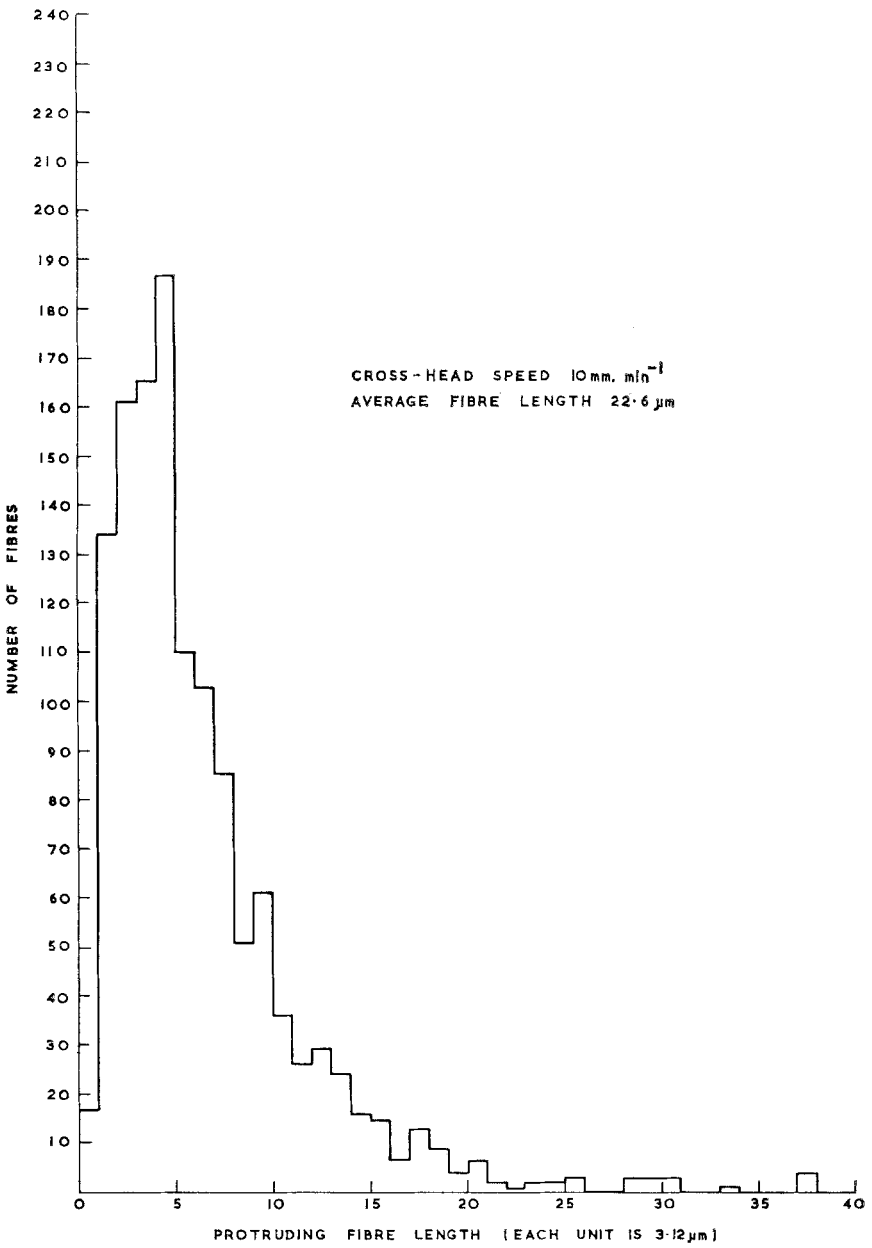

Figure 11

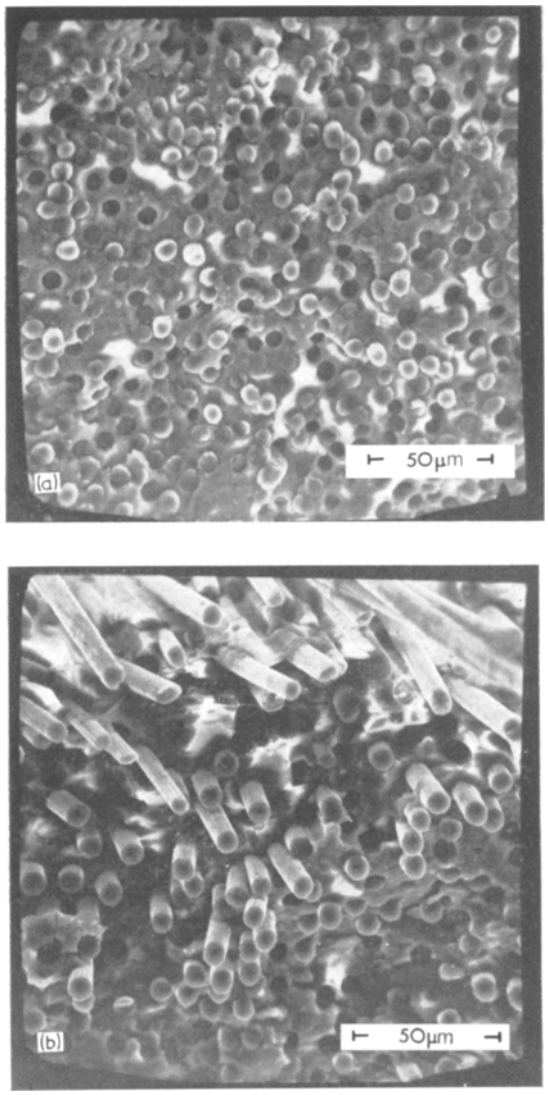

Figure 12 The fracture surface of an un-notched specimen (a) near the onset of failure (b) near the end of failure.

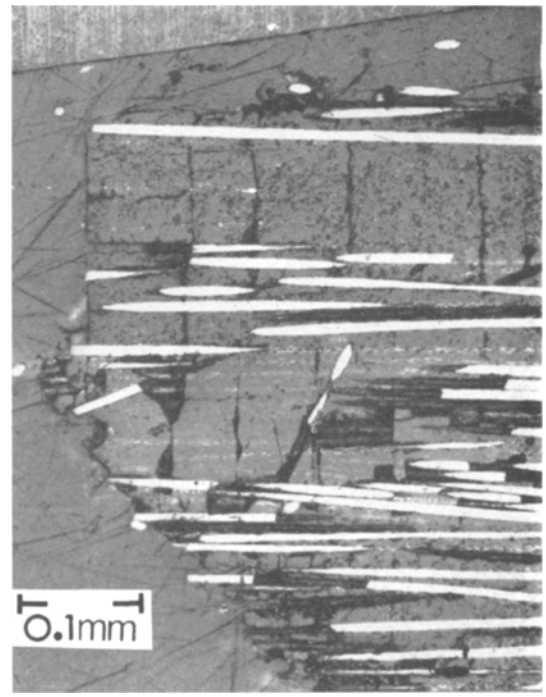

Figure 13 Matrix microcracking.

TABLE IV Fracture initiation energies (γ_I) at different notch depths

Notch depth (mm)	γ_I (kJm^{-2})	
	Fracture-mechanics analysis	Compliance analysis
0	—	—
1	1.5	1.4
2	1.0	0.8
3	0.8	0.4
4	0.5	0.3

isotropic materials of this geometry and the work of Sih *et al* [6] and Wu [10] has shown that such solutions can be applied to fibre composites for fracture in the principal symmetry directions. γ_I has been calculated from the fracture-mechanics analysis of Gross and Strawley [4, 11], using an effective modulus E_{eff} of 55 GNm^{-2}, and also a compliance analysis [4, 7], using the data in Fig. 6 and Table II. These techniques yielded the values shown in Table IV which average approximately 0.8 kJm^{-2}. These values are not considered very accurate because in most of the specimens the cracks did not initially propagate in a direction perpendicular to the fibres, but at a variety of angles between perpendicular and parallel. Further, the machined notches were not the sharp cracks that are required for accurate γ_I measurements. However, these two faults tend to counteract each other. The values of γ_I tend to decrease with increasing notch depth and the reasons for this are not obvious. It was noted that as notch depth was increased, there was a tendency for the crack to propagate at smaller angles to the fibre direction and thus it might be supposed that the lower values of γ_I are due to the crack initially propagating in lower energy directions. However, a similar variation of γ_I has been observed in boron-epoxy composites

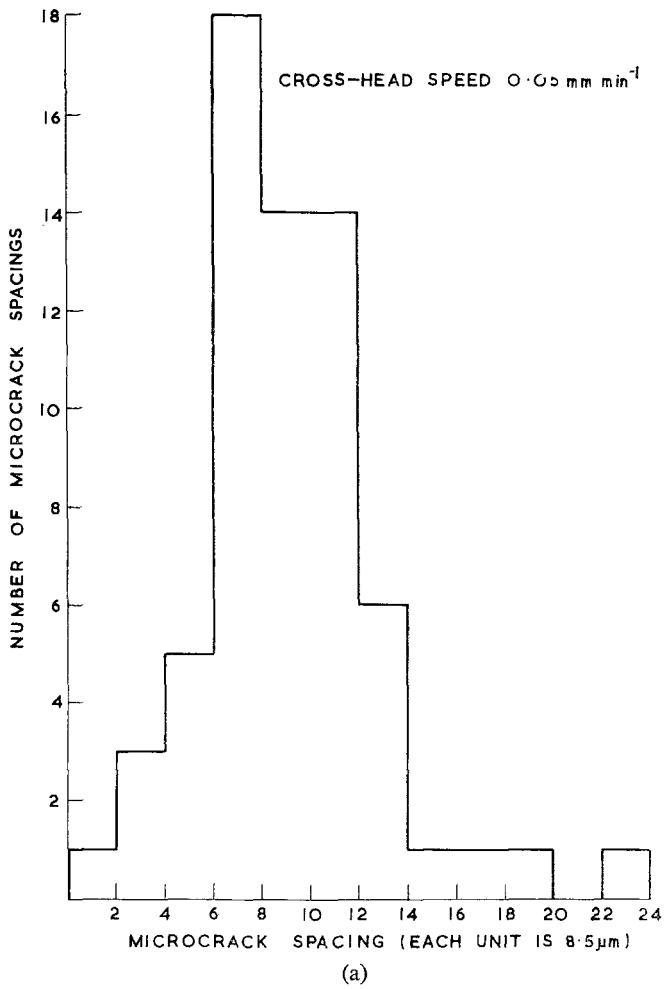

Figure 14 Histograms of microcrack spacings.

[12, 13], in which there was no deviation of the crack from the direction perpendicular to the fibres.

In the above calculation, an effective elastic modulus (E_{eff}) of 55 GNm^{-2} has been used because of the elastically anisotropic nature of the material. For isotropic materials, the appropriate value of modulus is the Young's modulus, but Sih *et al* [6] have shown that in general stress intensity factors are related to fracture energies by more complicated functions of the elastic constants which reduce to the Young's modulus in the special, isotropic case. The general conclusions of Sih *et al* and the calculation of the effective modulus used here are described in an Appendix.

4.3. The fracture process

The results suggest that fracture is initiated by a process whose energy is not the same as that for propagation. The initiation energy γ_I of a 40 vol % specimen is ~ 0.8 kJm^{-2} and is strain-rate independent within experimental error,

while the propagation energy is more accurately known as being about 3 kJm^{-2} for a similar specimen, this value being strain-rate dependent.

It is not surprising that the energies for initiation and propagation should be different in a fibre composite. When the composite is loaded in tension parallel to the fibres, fracture initiates when fibres snap within a distance $l_c/2$ of the composite fracture plane where l_c is defined as the minimum length of fibre which can be loaded to failure in a composite. At this instant, the load-bearing ability of the material will decrease. However, as in general the fibres do not break at the matrix fracture surface, the load-bearing capacity is not reduced to zero and additional work is done in pulling the fibres out of the matrix. It is postulated that the fracture initiation energy γ_I is largely the energy corresponding to the initial fibre failure and it is this energy which is relevant to fracture mechanics analyses, while γ_F, obtained from work of fracture, includes γ_I and the extra work done γ_P in pulling out fibres during the total separation of the fracture surfaces. In the case of CFRG, the propagation energy is larger than the initiation energy.

An approximate theoretical estimate of γ_I may be made by considering the initial rate of strain energy release during the fracture of fibres in a composite. Immediately before any continuous fibre snaps, the tensile stress in the fibre will be constant along its length at its fracture stress σ_f. When the fibre snaps, the stress is reduced to zero at the broken ends and increases to σ_f over a distance $l_c/2$ from each end. If it is assumed that the tensile stress builds up linearly from the broken end the difference in stored elastic energy in that fibre before and after its failure is then

$$\frac{\pi r^2 \sigma_f^2 l_c}{3E_f} \tag{2}$$

where r is the fibre radius and E_f is its Young's modulus. For a fibre-volume fraction V_f, the total energy release per unit area of cross-section due to this mechanism is

$$\frac{V_f \sigma_f^2 l_c}{6E_f} \tag{3}$$

and to this must be added $V_f \gamma_f$ where γ_f is the fracture energy of a fibre. Thus,

$$\gamma_I \sim \frac{V_f \sigma_f^2 l_c}{6E_f} + V_f \gamma_f \tag{4}$$

In order to evaluate this expression, it is necessary to have some estimate of l_c. This critical transfer length is determined by the distribution of shear stresses along the fibre-matrix interface and is therefore not necessarily the same before and during pull-out; and an estimate of it before pull-out may be obtained by considering matrix microcracking. In general, the shear stress at the fibre-matrix interface of a broken fibre is a maximum near the fibre end and decreases along the fibre. If the distance along the fibre axis from the broken end is x, then the shear stress is $\tau(x)$. A fibre of strength σ_f and radius r must then be greater than a length l_c if it is to be loaded to failure, and l_c is defined by

$$\int_0^{l_c/2} \tau(x)\, dx = \frac{\sigma_f r}{2} \tag{5}$$

Similarly, if a fibre is partially embedded in a matrix and a force is applied to its free end, the shear stress is a maximum where the fibre enters the matrix and decreases along the fibre as some function $\tau'(x)$. The condition that matrix microcracks should have a spacing t is [8]

$$\int_0^t \tau(x)\, dx = (\sigma_m)_u \frac{(1 - V_f)}{V_f} r \tag{6}$$

where $(\sigma_m)_u$ is the tensile strength of the matrix. In order to evaluate l_c from these expressions, it is necessary to know $\tau(x)$ and $\tau'(x)$. In the absence of a knowledge of these functions, an approximate value may be obtained by assuming that τ is constant. Then, by combining Equations 5 and 6,

$$l_c = \frac{\sigma_f t V_f}{(\sigma_m)_u (1 - V_f)} \tag{7}$$

The tensile strength of the matrix $(\sigma_m)_u$ can be estimated from the bend-over in the load-deflection curves of flexural specimens [8] and is shown as a function of strain-rate in Table V. The calculated values of l_c at the two strain-rates are 322 ± 22 μm at 0.05 mm min^{-1}, and 274 ± 40 μm at 20 mm min^{-1}, which are constant within experimental uncertainty. For carbon fibres $\sigma_f \sim 2000$ MNm^{-2} and $E_f \sim 360$ GNm^{-2}; for graphite $\gamma \sim 50$ Jm^{-2}; and for CFRG prior to fracture it has been shown that $l_c \sim 300$ μm. Inserting these values into Equation 4 for a 40 vol % composite of CFRG, leads to a value of γ_I of ~ 0.25 kJm^{-2}. This is a lower bound value as it assumes each fibre fractures just once, and is strain-rate independent as σ_f, the strength of carbon fibre is strain-rate independent [14] and l_c is constant within experimental uncertainty.

TABLE V Matrix tensile strengths and microcrack spacings at two strain-rates (uncertainties are standard errors)

Cross-head speed (mm min^{-1})	Matrix tensile strength (MNm^{-2})	Microcrack spacing (μm)
0.05	370 ± 8	89 ± 6
20	436 ± 35	90 ± 12

The dependence of pull-out energy ($\gamma_P = \gamma_F - \gamma_I$) on strain-rate is due to the dependence of the interfacial shear stress during pull-out on strain rate. This is further reflected in the variation of mean length of fibre protruding from the fracture faces.

The work of fracture data can be analysed to yield values for the interfacial shear stress which opposes the pull-out of fibres and leads to the high works of fracture. The work done in pulling out a fibre of embedded length l_i against a constant restraining shear stress τ, is,

$$W(l_i) = \pi r \tau l_i^2 \tag{8}$$

and the work of fracture of a composite, due to pull-out is

$$\gamma_P = \sum N_i W(l_i) \tag{9}$$

where N_i is the number of fibres of embedded length l_i. The histograms in Fig. 11 are representative samples of the distribution of l_i and, by combining Equations 8 and 9,

$$\tau = \frac{2r\gamma_P}{V_f} \frac{\sum N_i}{\sum N_i l_i^2} \tag{10}$$

where N_i and l_i may be obtained from the histograms. τ has been calculated from the data of LP355 by subtracting γ_I from γ_F to give γ_P, and the results are shown in Table VI. The restraining shear stress during the pull-out process varies from 16.5 MNm^{-2} at a cross-head speed of 0.05 mm min^{-1} to 32.6 MNm^{-2} at a cross-head speed of 10 mm min^{-1}.

The large variation of this interfacial shear stress would be expected to lead to a similar large variation in the critical transfer length l_c' during pull-out of a fibre in a composite. This is reflected in the lengths of fibres protruding from the fracture face. In general, the lengths of fibres protruding from a fracture face will vary from zero to $l_c'/2$ where l_c' varies from fibre to fibre and along the length of any fibre due to the distribution in the strength of the fibres. In general, the mean length of protruding fibre will be approximately $\overline{l_c'}/4$. For a constant shear stress along the fibre-matrix interface.

$$l_c' = \frac{\sigma_f r}{\tau} \tag{11}$$

and thus the mean length of protruding fibre varies inversely as τ. Table VI shows this to be the case and shows the shear stresses calculated from Equation 11, assuming a strain-rate independent value of σ_f of 2000 MNm^{-2}. These calculated shear stresses are close to these obtained from the work of fracture values.

It is not clear why the interfacial shear stresses during pull-out should be so sensitive to strain-rate. Some strain-rate dependence is to be expected because of the strain-rate dependence of the strength of glass. However, the tensile strength of the matrix varied by only about 15% during these experiments, while the interfacial shear stress during pull-out varied by ~ 100%. In order to explain this effect, and also to more accurately calculate the theoretical value of γ_I it will be necessary to study the nature of the fibre-matrix interface in more detail, and in particular, to determine how the shear stress varies along the interface during loading.

5. Conclusions

(a) The work of fracture technique yields meaningful material properties only when crack propagation is completely controlled throughout failure.

(b) Work of fracture is strain-rate sensitive and decreases with increasing strain-rate. It increases with fibre volume fraction and was typically about 3 kJm^{-2} for a 40 vol% composite. Fracture initiation energies are less than works of fracture and no strain-rate sensitivity has been detected. The initiation energy of a 40 vol% composite was approximately 0.8 kJm^{-2}.

TABLE VI Interfacial shear strengths (τ) during pull-out

Cross-head speed (mm min^{-1})	Work of fracture (γ_F) (kJm^{-2})	Pull-out energy (γ_P) (kJm^{-2})	$\frac{\Sigma N l^2}{\Sigma N}$ (μm)^2	Mean length of fibre $\bar{l}_i = \bar{l}_c'/4$ (μm)	τ from γ_P (MNm^{-2})	τ from $\bar{l}_i$ (MNm^{-2})
0.05	3.1	2.3	2955.3	44.1	16.5	18.2
0.5	2.6	1.8	1415.4	30.2	25.5	26.7
10	2.1	1.3	802.3	22.6	32.6	35.4

(c) The fracture initiation energy has been explained in terms of the immediate release of strain energy during fibre fracture. The theoretically estimated initiation energy of a 40 vol % composite is about 0.25 kJm^{-2} which is lower than the experimental value, but the strain-rate insensitivity is predicted theoretically.
(d) The interfacial shear stress during pull-out is dependent on strain-rate, varying from 16.5 to 32.6 MNm^{-2} in these experiments.
(e) More accurate measurements of γ_I are required, and it will be necessary to study in some detail the fibre-matrix interface and the shear stress distribution along it before γ_I and γ_F can be understood properly.

Acknowledgements

This work was carried out partly in the Materials Development Division at AERE, Harwell, and partly in the Materials Department of the University of California at Los Angeles. I am grateful to my colleagues at both of these places for their interest and assistance. In particular I thank Dr A. S. Tetelman and Dr P. W. R. Beaumont for several helpful discussions, and Miss S. Kunz for assistance with the experimentation.

Appendix

Fracture mechanics analysis of elastically anisotropic materials

Sih *et al* [6] have shown that the stress intensity factors of elastically anisotropic materials are identical to those of isotropic materials. Thus, the opening mode, stress intensity factor, k_1, for a crack of length $2c$ in an infinite body under a tensile-stress applied at an angle α to the crack, and of magnitude σ^∞ a long distance away is

$$k_1 = \sigma^\infty c^{\frac{1}{2}} \sin^2\alpha \qquad (1)$$

The stress intensity factor is in general related to the strain-energy release-rate G_{1c} for the opening mode by

$$G_{1c} = \pi k_{1c}^2 \left(\frac{a_{11}a_{22}}{2}\right)^{1/2} \left[\left(\frac{a_{22}}{a_{11}}\right)^{1/2} + {}^2\left(\frac{a_{12} + a_{66}}{2a_{11}}\right)\right]^{1/2} = \frac{\pi k_{1c}}{E_{eff}} \qquad (2)$$

where a_{ij} are components of the material's compliance matrix, the crack lying parallel to the 1-axis and perpendicular to the 2-axis.

For an isotropic material

$$a_{11} = a_{22}$$
$$a_{66} = 2(a_{11} - a_{12}) \qquad (3)$$

and thus

$$G_{1c} = \pi k_{1c}^2 a_{11} = \frac{\pi k_{1c}^2}{E} \qquad (4)$$

where E is Young's modulus.

In the case of a crack under a perpendicular stress, this leads to the well-known Griffith equation, $\sigma^\infty = (EG_{12}/\pi c)^{1/2}$.

The simple relationships of Equations 3 do not hold true for anisotropic materials and it is then necessary to know the components of the compliance matrix. These have not been measured off carbon-fibre reinforced glass, however Tsai [15] has demonstrated how they may be calculated theoretically from a knowledge of elastic constants of the fibres and matrix separately. Using Tsai's formulae, and data which he has supplied for carbon-fibre and glass, the compliance matrix has been calculated for a 40 vol % carbon fibre-glass composite in which the fibres are parallel to the 2-axis.

This, in units of $(10^3\ GNm^{-2})^{-1}$, is

19.4	82.0	133.0	0	0	0
	6.10	82.0	0	0	0
		19.4	0	0	0
			31.7	0	0
				45.5	0
					31.7

It follows from Equation 2, that E_{eff} in Equation 2 is 55.0 GNm^{-2}.

References

1. H. G. TATTERSALL and G. TAPPIN, *J. Mater. Sci.* **1** (1966) 296.
2. R. A. J. SAMBELL, D. H. BOWEN, and D. C. PHILLIPS, *ibid* **7** (1972) 663.
3. R. A. J. SAMBELL, A. BRIGGS, D. C. PHILLIPS, and D. H. BOWEN, *ibid* **7** (1971) 676.
4. R. W. DAVIDGE and G. TAPPIN, *ibid* **3** (1968) 165.
5. JUNN NAKAYAMA, *J. Amer. Ceram. Soc.* **48** (1965) 583.
6. G. C. SIH, P. C. PARIS, and G. R. IRWIN, *J. Fracture Mechanics* **1** (1965) 189.
7. See for example, H. T. CORTEN, in "Modern Composite Materials", L. J. Broutman and R. H. Krock (Eds.) (Addison-Wesley, Reading, Massachusetts, 1967) p. 44.
8. D. C. PHILLIPS, D. H. BOWEN, and R. A. J. SAMBELL, *J. Mater. Sci.* to be published.
9. D. H. BOWEN, D. C. PHILLIPS, R. A. J. SAMBELL, and A. BRIGGS, 1971, International Conference on the Mechanical Behaviour of Materials, Kyoto, Japan (Society of Materials Science, Japan).

10. EDWARD M. WU, T and AM Report No. 248, University of Illinois, 1963.
11. B. GROSS and J. E. SRAWLEY, reported in ASTM, STP410, 1966.
12. J. M. FITZ-RANDOLPH, M.S. Thesis, Materials Department, School of Ehgineering and Applied Science, UCLA, 1971.
13. J. M. FITZ-RANDOLPH, D. C. PHILLIPS, P. W. R. BEAUMONT, and A. S. TETELMAN, "Work of Fracture and Acoustic Emission Studies of a Boron-Epoxy Composite", Fifth St Louis Symposium on Advanced Composites, St Louis, Missouri, 1971.
14. E. DELAMOTTE and A. J. PERRY, *Fiber Sci. and Tech.* **3** (1970) 157.
15. STEPHEN W. TSAI, "Formulas for the Elastic Properties of Fiber-Reinforced Composites", (Monsanto/Washington University, ONR/ARPA Association, HPC68-61, 1968).

Received 9 March and accepted 22 March 1972.